4-12-2022

Surface Urban Heat Island in South Korea's New Towns with Different Urban Planning

Kyungil Lee
Korea University - Korea

Yoonji Kim
Korea University - Korea

Hyun Chan Sung
Korea University - Korea

Seung Hee Kim
Chapman University, sekim@chapman.edu

Seong Woo Jeon
Korea University - Korea

Recommended Citation

Lee, K., Kim, Y., Sung, H.C. et al. Surface urban heat island in South Korea's new towns with different urban planning. *Environ Monit Assess* 194, 360 (2022). https://doi.org/10.1007/s10661-022-09967-w

Surface urban heat island in South Korea's new towns with different urban planning

Kyungil Lee[1], Yoonji Kim[1], Hyun Chan Sung[1], Seung Hee Kim[2] and Seong Woo Jeon[1,*]

[1]Division of Environmental Science & Ecological Engineering, Korea University, 145, Anam-ro, Seongbuk-gu, Seoul 02841, Republic of Korea
[2]Center of Excellence in Earth Systems Modeling and Observations, Chapman University, Orange, CA 92866, USA

* Corresponding author at Division of Environmental Science & Ecological Engineering, Korea University, 145, Anam-ro, Seongbuk-gu, Seoul 02841, Republic of Korea.
E-mail address: eepps_korea@korea.ac.kr (Seong Woo Jeon)

Abstract: A new town is strategically built within a short period compared to naturally developed cities. It is considered as an appropriate study area for analyzing the urban climate problems such as Surface Urban Heat Islands (SUHIs) that is differently generated according to urban planning and development. In this study, we suggest comprehensive method for determining and comparing changes in surface UHI distribution during 1989–2048 in two new towns with different urban planning. First, a substantial increase in built-up areas was observed from 1989 (< 5%) to 2018 (> 40%) in both new towns. However, SUHI phenomenon increasing patterns were different of about 12.25% depending on urban planning and urban morphology. Results also showed the importance of vertical and horizontal structures which can have a great influence on SUHI intensity and accordingly, the difference in SUHI distribution between two new towns was confirmed. Moreover, without effective mitigation, the built-up area in both new towns are estimated to increase to approximately 60%, and the SUHI intensity in most areas to increase by 4 °C in 2048. In addition, the spread and intensification of the SUHI phenomenon are predicted to be greater due to the characteristics of the building structure and the active urban expansion. Thus, these results combined with architectural assessment models can improve the understanding of thermal environmental impacts of urbanization and provide directions for sustainable urban development and renovation.

Keywords: Urban heat island, Land use land cover change, CA-Markov model, Remote sensing, Urban planning

(9671 words)

1. Introduction

Global population growth and urban expansion primarily cause land use and land cover (LULC) changes and increases in built-up area. In 2018, approximately 55.3% of the world's population resided in cities, among which 60% will reside in cities with approximately 0.5 million inhabitants by 2030 (UN, 2018). Rapidly increasing economic development accelerates these changes, particularly in fast-growing urban areas, hindering sustainable development (Liping et al., 2018). LULC changes induced by human activities lead to different local climates than in surrounding areas. This effect, termed as urban heat island (UHI), occurs worldwide (Eliasson, 2000; Lee et al., 2020). UHIs primarily occur due to increased solar radiation absorption and trapping in new surface materials of various infrastructure (Grimmond, 2007; Santamouris, 2013). The magnitude and extent of UHIs are highly positively correlated with urban area and population size in cities; thus, UHIs are significantly affected by urban expansion (Tran et al., 2006). UHIs can be divided into two types: meteorological UHI, an increase in local air temperature, and surface urban heat island (SUHI), an increase in urban skin temperature. SUHI is particularly evident in spatial variations of upwelling thermal radiance caused by LULC changes and is commonly influenced by the surrounding sub-urban environment (Clinton & Gong, 2013; Voogt & Oke, 2003). Hence, accurate analysis of LULC changes and mapping of ongoing land changes are crucial to understanding its effects on urban climate and can support policymakers in environmental management (Cetin, 2019).

A new town, also called planned city, is built in a short period within a pre-determined boundary for specific purposes. Since the mid-to-late twentieth century, new towns have been constructed worldwide, contributing to population growth and inflation in large cities (Wakeman, 2016). A planned city is a fertile ground for Microclimate research, offering the opportunity to formulate urban planning strategies to solve problems like UHIs (Qaid et al., 2016). Environmental conditions such as ecological balance and thermal comfort have become important factors for choosing the cities to live in (Cetin, 2019). Comparing and evaluating different planned urbanization could provide a rich source of knowledge on the effects of the urban environment changes on the long-term temperature trends in the urban area (Cetin, 2015). However, few studies have compared the UHI phenomenon between new towns having different urban planning. Carrying out comparative studies on climate effects of urbanization under different urban planning conditions is particularly difficult because of different urban environments, economic situations, and climates, as well as inconsistent data.

Since 1990, 16 new towns have been repopulated or built in sub-urban areas in South Korea to manage population, transportation, and environmental concerns in several large cities. Urban planning in the first-generation new towns, providing indiscriminate housing, was not systematic and resulted in negative impacts, such as unplanned urban expansion, environmental degradation, and low greenspace ratio in housing complexes. The second-generation new towns were developed through systematic and environmentally friendly urban planning, such as low-density urbanization and expansion of green areas. However, in both cases, an increase in SUHI is estimated because of a rapid infrastructural development and vegetation loss. Moreover, the SUHI phenomenon may intensify with further urban expansion.

Herein, expansion and intensification of SUHI due to new towns development were empirically analyzed using satellite data in two new towns with different urban plannin in South Korea. The SUHI intensity of each new town is the difference between the temperatures of built-up and surrounding areas within the boundary (Guha et al., 2018; Lee et al., 2020; Oke et al., 2017; Zhou et al., 2013). A Markov chain model, combined with the cellular automata method, determined the SUHI distribution with LULC changes in the two new towns. Notably, urban planning influenced the change patterns in the expansion and intensification of UHIs, despite urban expansion. Furthermore, the future SUHI intensities in new towns may significantly increase with changes in structural characteristics owing to renovation and additional urban expansion.

2. Datasets and methods

2.1 Study Area

The study areas are Bundang and Pangyo new towns in South Korea. In the case of South Korea, 16 new towns have been in the repopulation phase or under construction in suburban areas since the 1990s to solve the problem of population, transportation, and environment concentrated in several large cities (Fig. 1).

The purpose of the first-generation new town was to supply housing indiscriminately, and urban planning was not systematic. As a result, negative problems such as unplanned urban expansion and damage to the natural environment, low greenspace ratio in the housing complex occurred. In the case of the second-generation new town, urban spaces were created based on systematic and environmental-friendly urban planning such as low-density urbanization and expansion of parks and green areas. Information on the two new cities was examined through related literature and information provided by the site (https://eiass.go.kr/) (Table 1). Compared to Bundang new town, Pangyo new town has a lower planned population and building density, lower floor space ratio and higher greenspace ratio. In addition, the ratio of non-apartment housing sites among the housing complexes to be developed is 36.4%, which is three times higher than that of Bundang new town. Therefore, it is expected that the spread of the SUHI phenomenon and the degree of increase in magnitude according to each new town development will be different by different urban characteristics and morphology. Although the total areas of the two new towns are different, the impact of urban planning can be confirmed through the difference in the rate of change.

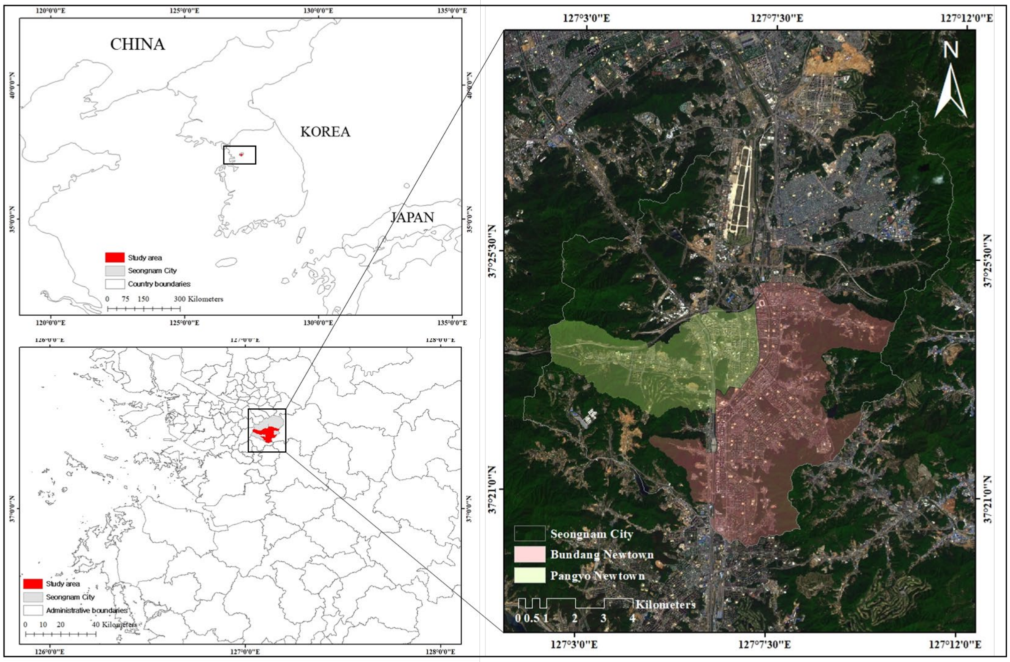

Fig. 1. Map of study area showing geographical location of two new towns with Landsat OLI image acquired on May 09, 2018.

Table 1

Development plan features for each new town.

Division (unit)	Bundang new town	Pangyo new town
Generation of the new town	1st generation	2nd generation
Development period	'89 ~ '96	'03 ~ '17
Development area (km^2)	19.64	8.9
Number of total household (thousands)	97.6	29.3
Number of apartment household (thousands)	10.6 (10.8%)	10.7 (36.4%)
Number of non-apartment household (thousands)	87.0 (89.2%)	18.6 (63.6%)
Population density (number / ha)	199	98
Average greenspace ratio (%)	12~25	25~35
Average floor space ratio (%)	184	161
Transportation infrastructure	Vehicle-oriented	Public transportation-oriented

2.2 Data acquisitions and pre-processing

We used three Landsat images taken in May with image quality of 9 and cloud cover less than 2% to minimize the seasonal influence and cloud cover of each period: 1989, 2000, 2018 (Table 2). Two Landsat 5 Thematic

Mapper (TM), and one Landsat 8 Operational Land Imager/Thermal Infrared Sensor (OLI/TIRS) images obtained from United States Geological Survey-Center for Earth Resources Observation and Science (USGS-EROS) (httl://earthexplorer.usgs.gov/). The specifications of the images are given in Table 2. Images were used for LULC classification and SUHI calculation and each period can show the change trends before and after the new town development.

The remotely sensed data is an indirect measurement requiring consideration of the interfering atmosphere and the surface radiative properties that affect the emission and reflection of radiation of within the spectral wavelengths detected by the sensor (Voogt & Oke, 2003). Atmospheric correction using Dark Object Subtraction (DOS) method and radiometric correction as preprocessing using Semi-Automatic Classification (SCP) plugin in QGIS 3.14 were applied to the images. Atmospheric scattering and absorption make imaging system record a non-zero digital number (DN) value for dark objects and DOS method subtracted continuous non-zero DN vale, DN haze from the whole band assuming that some objects were under comprehensive shadow must have zero reflectance (Nazeer et al., 2014).

Table 2

Characteristics of collected images.

Study Period	Sensor	Acquisition Date	Resolution	Cloud Cover	Path / Row
1989	Landsat 5 TM	18 May 1989	30m	0.00%	115 / 34
2000	Landsat 5 TM +	07 May 2000	30m	0.00%	116 / 34
2018	Landsat 8 OLI	09 May 2018	30m	1.22%	116 / 34

2.3 Land use land cover classification (LULC)

2.3.1 Maximum Likelihood Classifier algorithm

We used supervised classification technique with Maximum Likelihood Classifier (MLC) algorithm to generate LULC maps of each year using SCP plugin in QGIS 3.14. The MLC based supervised classification approach was comprehensively used and considered as a proven technique in many previous studies for urban LULC classification where spatial conglomeration of pixels so high (Saha et al., 2020; Sun et al., 2013; Wang et al., 2021). MLC algorithm is based on the probability density distribution functions (likelihood) including all training inputs for each land cover class and proven to be more accurate, robust algorithm because it does not overvalue the class values during the computational process. In addition, there are some advantages of the MLC algorithm, (1) auto-allocation of pixels to the unclassified regions based on the surrounding values, (2) variance and covariance values of the class signatures are considered within the class distribution (Erbek & Taberner, 2004), etc.

The Landsat images of 1989, 2000, 2018 were classified into six LULC classes, (i) built-up areas, covering the buildings and concrete areas, (ii) forest, covering coniferous forest and broadleaf forest, (iii) grass, covering natural grass and artificial grass, (iv) open spaces, covering natural bare areas and artificial bare areas, (v) agricultural areas, covering paddy field, dry field, etc, (vi) water bodies, covering ponds, lakes, wetlands.

2.3.2 Accuracy assessment

Assessment of classification accuracy is necessity for classification data to detect changes and was carried out on the resulting classified imagery through error matrix and kappa index that allows differentiating between ground-truth and predicted classification (Lee et al., 2020). High resolution Google Earth data and aerial photograph provided by National Geographic Information Institute (NGII) of South Korea were used to ascertain ground-truth regions for evaluation of classification accuracy (http://map.ngii.go.kr/). Google Earth's high-resolution data have been used as reference data in many classification studies and national standardized land cover map and NGII has provided high-resolution aerial photograph taken since 1945, it can be used for accuracy assessment as well (Lee et al., 2020; Saha et al., 2020). Kappa coefficient was estimated using equation (1):

$$Kappa-coefficient = \frac{n\sum_{i=1}^{k} nii - \sum_{i=1}^{k}(G_i C_i)}{n^2 - \sum_{i=1}^{k}(G_i C_i)} \quad (1)$$

Where i is the class number, n is the total number of points, nii is the number of pixels of actual data class i, that were classified as a class i, Ci is the overall number of classified pixels belonging to class i and Gi is the overall number of actual data belonging to class i. 50 samples points per class for each new town except water class has been selected automatically by QGIS 3.14. It is recommended that a minimum of 50 samples for each land cover class in the error matrix be collected for the accuracy assessment to avoid risk of a biased sample (Congalton, 1991).

2.4 LST estimation

Land surface temperature (LST) estimation using ArcMap 10.5 consists of the transformation of digital numbers (DN) to radiances (L_λ), the measurement of radiance brightness-temperatures (TB) and the adjustment of emissivity to extract surface temperature from brightness maps (Avdan & Jovanovska, 2016). LST were obtained using thermal band from Landsat ETM+ (B6) and Landsat OLI/TIRS (B10) because of suggestions of USGS of not using TIRS band 11 due to its higher calibration uncertainty.

Every object in earth radiates its thermal electromagnetic radiation after its temperature is above absolute zero (K) and the signal obtained by the thermal sensors could be transformed to radiances (L_λ) using equation (2):

$$L_\lambda = M_L \times Q_{CAL} + A_L \quad (2)$$

Where L_λ = spectral radiance (W/(m^2*sr*μm)); ML = radiance multiplicative scaling factor for the band; A_L = radiance additive scaling factor for the band; and Qcal = level 1 pixel value in DN and the metadata of the Landsat images provide their values. After the DN are converted to radiance, radiance values were converted into brightness temperature TB using equation (3):

$$T_B = K_2/\ln[(K_1/L_\lambda) + 1] - 273.15 \quad (3)$$

Where T_B = At-satellite brightness temperature; K_1 and K_2 stand for the band-specific thermal conversion constants from the metadata and for obtaining the temperature in Celsius, the radiant temperature is revised by adding the absolute zero (Avdan & Jovanovska, 2016). The last step of estimating the LST is to rectify brightness temperature by Land Surface Emissivity (LSE, ε) correction using equation (4) (Artis & Carnahan, 1982):

$$LST = \frac{T_B}{[1 + [\frac{\lambda \times T_B}{\rho}] \times \ln\epsilon]} \quad (4)$$

Where λ is wavelength of emitted radiance (≒ 10.895μm); ρ = h × (c/σ), where h is Planck's constant (6.626 × 10-34Js, c is the velocity of light (2.998 × 10^8m/s), and σ is the Boltzmann constant (1.38 × 10-23J/K); ε is the emissivity (Avdan & Jovanovska, 2016; Weng et al., 2004).

Obtained values of T_B were referenced as a black body, which is different from properties of real objects on the Earth's surface, and it would be different with real LST (Shen et al., 2016). The magnitude of the LST range across a city could be extremely huge and it depends on LULC states constructed within the city and LSE which is essential for estimating the LST has strong land use/land cover dependence (Mallick et al., 2012; Rhadi et al., 2013). The determination of the LSE is calculated conditionally as proposed by Sobrino et al (2004) using equation

(5) and the emissivity value is represented with the formula for each condition based on Normal Difference Vegetation Index (NDVI) range (Wang et al., 2015) (Table 3):

$$\epsilon_{\lambda} = \epsilon_{\lambda v} P_v + \epsilon_{\lambda s}(1 - P_v) + C_{\lambda} \quad (5)$$

Table 3

NDVI ranges and corresponding formula for calculating emissivity value.

NDVI range	**Emissivity value**
$NDVI < NDVI_S$	$0.979 - 0.046_{\rho R}$
$NDVI_S \leq NDVI \leq NDVI_V$	$\epsilon_{\lambda} = \epsilon_{\lambda v} P_v + \epsilon_{\lambda s}(1 - P_v) + C_{\lambda}$
$NDVI > NDVI_V$	0.99

Visible Red (λ-0.6μm) and Near-Infrared, NIR (λ-0.8μm) bands were used for calculating NDVI using equation (6). NDVI values range from +1.0 to -1.0 and is correlated with physical properties of the vegetation canopy and fractional vegetation cover. Where εv and εs are the vegetation and soil emissivity individually and C_{λ} is the surface roughness ($C_{\lambda} = 0$ for homogeneous and flat surface) taken as a constant value of 0.005 (Sobrino & Raissouni, 2000). When the NDVI is less than $NDVI_S$ (=0.2), it is classified as bare soil and the emissivity value is acquired from the reflectance values in the red region (ρR) (Seketekin & Bonafoni, 2020). For NDVI values between 0.2 and 0.5 are considered as mixtures of soil and vegetation surface and equation (10) is used for extracting emissivity values. Where $\varepsilon_{\lambda v}$ is emissivity value of vegetation in this range (≒ 0.9863μm) and $\varepsilon_{\lambda s}$ is emissivity value of soil in this range (≒ 0.9668μm) (Yu et al., 2014). When the NDVI value is larger than NDVIv (=0.5), it is considered as vegetation surface and the value of 0.99 is assigned (Avdan & Jovanovska, 2016). In addition, NDVI value were used for calculating the proportion of the vegetation (Pv) related with emissivity (ε) using equation (7) (Carlson & Ripley, 1997; Tucker, 1979). A method for calculating Pv is suggests using the NDVI values for vegetation soil to apply in global conditions (Sobrino et al., 2004).

$$NDVI = \frac{NIR - RED}{NIR + RED} \quad (6)$$

$$P_V = \left[\frac{NDVI - NDVI_S}{NDVI_V - NDVI_S}\right]^2 \quad (7)$$

2.5 Prediction analysis

2.5.1 Urban expansion prediction

We used integrated Cellular Automata (CA) – Markov Chain Model (MCM) for prediction of 2028, 2038, 2048 urban expansion scenario of two new towns. CA-Markov chain model is hybrid and robust algorithm in spatial and temporal dynamic modelling of LULC changes that includes the deterministic modelling framework, spatially specific methodology with stochastically based temporal structure (Kamusoko et al., 2009; Keshtkar & Voigt, 2016).

MCM is a tool to evaluate adjustments in land use among cycles by a sequence of values that depend on present state (Aaviksoo, 1995). MCM defines the LULC change from one time to another to predict future change and equation (8) explains the calculation of the prediction of land use change (Kumar et al., 2014):

$$S(t, t+1) = Pij \times S(t) \quad (8)$$

Where S(t) is the system state at time of t, S (t+1) is the system state at time of t+1; Pij is the transition probability matrix in a state which is established using equation (9):

$$P_{ij} = \begin{vmatrix} P_{1,1} & P_{1,2} & \cdots & P_{1,N} \\ P_{2,1} & P_{2,2} & \cdots & P_{2,N} \\ \cdots & \cdots & \cdots & \cdots \\ P_{N,1} & P_{N,2} & \cdots & P_{N,N} \end{vmatrix} \quad (0 \le P_{ij} \le 1) \quad (9)$$

P is the Markov probability matrix, and P_{ij} represents the probability of converting from current state i to another state j in prediction time; PN is the state probability of any time. Low transition pixel will have a low probability value near (0) and high transition pixel have high probability value near (1). The 2000 LULC map of the study area was used as the base (t1) and 2018 LULC map was used as the later (t2) to obtain the transition probability matrix in this study

CA is a dynamic procedure model that is used for the land use cover change (Hamad et al., 2018). CA has capability to change its state according to a rule that each cell with their own characteristics can stand for parcels of land and self-growth interactions as they are dynamic and reduplicate (Brown et al., 2004). Hence, the CA-MCM which integrate the theories of Markov with CA, is about the time series and space for the improvements for forecasting and can attain better simulation for temporal and spatial patterns of land use changes (Sang et al., 2011).

Multi-Criteria Evaluation (MCE) was used to decide which LULC classes are appropriate for changing from original state to another. MCE combines driving factors for urban growth and fuzzy systems analysis to construct transition suitability maps which show the probability of a pixel to change to another land cover class or be unchanged. (Myint & Wang, 2006). Physical planning and transportation infrastructure for the new town planning is important for large-scale development to create housing sites within a short period of time. Transportation is especially believed to accelerate and guide urban expansion via the improvement of accessibility (Anas et al., 1998; Hu & Lo, 2007; Kasraian et al., 2019). In addition, Slope is an uncontrollable environmental factor that affects urban growth; construction of buildings and development of cities on steep-slope terrain has been problematic or impossible (Kechebour, 2015). Hence, distance to main road, slope, and distance to existed urban area were used in estimating transition suitability maps in this study. The maps of road, Digital Elevation Model (DEM) were obtained from National Spatial Data in Infrastructure Portal (NSDIP) (http://data.nsdi.go.kr/). Fuzzy membership functions were used to standardize suitability maps into 0-1, where 0 represents inappropriate locations and 1 represents suitable locations for urbanization. The future assignment to LULC class for each cell was based on how much the cell is appropriate for LULC class and how close the cell is to neighboring cells of the same class and contiguity filter of 5×5 pixels was used to identify the effect of neighboring pixels on the central pixel.

2.5.2 Mapping and prediction of SUHI distribution

The UHI phenomenon results from the anthropogenic modification of natural landscapes in the city boundary layer and as the urban area increases, the UHI intensity also increases (Oke, 2002). In addition, LST and SUHI effects are especially relative to the surrounding ex-urban environment (Clinton & Gong, 2013). To reflect this trend, I defined the SUHI intensity of each new town as the difference between temperatures of an urban area and suburban areas (LULC excluding built-up area) within the boundary (Guha et al., 2018; Lee et al., 2020; Zhou et al., 2013). Based on this concept, the SUHI intensity distribution maps for each new town and each period were constructed using two techniques: (1) to calculate SUHI intensity variation using equation (10):

$$\text{SUHI intensity distribution} = T_s - (T_{mean} + 0.5\times\delta)_{\text{surrounding area}} \quad (10)$$

Where Ts is LST (°C) distribution of new town, T mean and δ are the mean and standard deviation of LST in non-urban areas of the new town. By subtracting the average temperature of non-urban areas from the temperature of the whole city, it is possible to confirm the actual SUH effect due to urban expansion rather than temporary LST value. In addition, I have excluded the water bodies while calculating SUHI intensity because it can change the LST irregularly (Lee et al., 2020). (2) to classify SUHI intensity variation into six appropriate ranges: (i) values ≤ 0℃, (ii) 0℃ < values ≤ 2℃, (iii) 2℃ < values ≤ 4℃, (iv) 4℃ < values ≤ 6℃, (v) 6℃ < values ≤ 8℃, (vi) 8℃ < values. In this way, it is possible to compare the difference in distribution and intensity of the SUHI phenomenon according to the change in LULC for each new town at each time. In addition, classes are divided according to the value range, so that future SUHI intensity distribution could be predicted using CA-Markov analysis. Indices positively and negatively correlated with LST were used to develop in calculating transition suitability maps for predicting SUHI distribution. Normalized Difference Built-up Index (NDBI) suggested by Zha et al. (2003) was used as index strongly correlated with LST. NDBI is the most used and commonly accepted method for the identification of built-up areas and showed a high surface temperature correlation in previous studies (Saha et al., 2020; Tariq & Shu, 2020). The NDBI is calculated using equation (11):

$$NDBI = \frac{SWIR - NIR}{SWIR + NIR} \tag{11}$$

Built-up areas are sensitive under 1.55-1.75 wavelength range in the Short-Wave Infrared (SWIR) band, whereas shows lower sensitivity under 0.79-0.90 wavelength range in NIR band (Bhatti & Tripathi, 2014). The NDBI values range from -1 to +1 and the values near to +1 normally represent highly dense built-up areas. NDVI was used as index weakly correlated with LST. NDVI is the most common index for vegetation detection and showed a strong negative correlation with LST in previous studies (Sun et al., 2015; Tariq & Shu, 2020; Weng et al., 2004). Fuzzy membership functions were also used to standardize factor maps into 0-1, where 0 represents low SUHI potential and 1 stand for high SUHI potential.

3. Results

3.1 LULC changes according to new towns development

In the accuracy assessment of the three LULC classifications, the kappa coefficient in LULC classification areas for all the three years were greater than 0.8, verifying that these classifications were significant predictors of future LULC and SUHI distribution.

LULC analysis show that the extent and proportion of LULC types varied across the years and I could observe the significant transformations between 1989 and 2018. The accumulation of built-up areas in the two new towns have been drastically extended during each development period (Fig. 2b and Fig. 3b). However, it was observed that forest and agricultural areas had significantly declined. In 1989, most of LULCs of Bundang new town and Pangyo new town were forest and agricultural areas, accounting for almost 13.90 km^2 (85%), and built-up areas were less than 5%. After that, the highest built-up growth was taken place in Bundang new town between 1989 and 2000 when the development of Bundang new town had already ended. The built-up areas increased from 1.47 km^2 (4.39%) to 14.09 km^2 (42.13%), however, agricultural areas drastically decreased from 13.90 km^2 (41.55%) to 2.99 km^2 (8.93%) and forest also considerably decreased from 44.19% to 33.88%. In addition, open spaces increased from 0.46% to 5.68%, which occurred due to the development of the new town or was confirmed as an area under development at the time (Fig. 2a). In the case of Pangyo new town, relatively little change occurred because the new town development planning was not yet established. In the case of built-up areas, the proportion was increased from 3.23% to 16.73%, which was confirmed by the construction of the main road within the boundary and the unplanned and fragmented development (Fig. 3a). It also appears to have increased the percentage of open spaces in this process.

In the case of 2018, when the development of Pangyo new town was completed, the proportion of built-up areas of Pangyo new town increased dramatically from 16.73% to 40.81%. Forest decreased from 46.36% to 40.84% and remaining agricultural areas decreased to 1.96%, resulting in almost all urbanization. In the case of Bundang new town, the increase in built-up areas between 2000 and 2018 was relatively small, but agricultural areas decreased to 1.71%, which also became almost urbanized. Open spaces of both new towns that existed in 2000 were mostly urbanized in 2018. In the case of grass, the overall area was similar, and the ratio of grass is higher in Pangyo new town as in the development plan. However, due to the limitation of resolution, grass existing inside the built-up areas could not be classified. Therefore, the actual ratio between the two new towns will be more different. In the case of water, there was no significant change in area between 1989-2018, but fluctuations due to spectroscopic differences were observed.

3.2 SUHI distribution changes according to new towns development

The accumulation of higher SUHI intensity areas in the two new towns have been extended according to urban area growth (Fig. 2d and Fig. 3d). In 1989, there were no areas in both Bundang and Pangyo new towns with a SUHI intensity of six or higher. Most of the areas with evident SUHI phenomenon were agricultural areas and partially urbanized areas. LST is vulnerable to vegetation mass, and in Korea, may is an early growing season in agricultural areas that contain less vegetation mass compared to the surrounding forest (Raymond et al., 1994). This difference in vegetation mass led to a high temperature distribution in agricultural areas in both new towns. In 2000, the area with SUHI phenomenon increased by approximately 30% after the development of Bundang new town. The areas with SUHI occurrence in the range of 2–4 ℃ significantly increased from 3.4 km^2 (10.18%) to 10.82 km^2 (32.34%), and those with more than 4 °C, which were few in 1989, increased to approximately 3.03 km^2 (9%) of the total area. Most of the areas with SUHI in the range 0-2 ℃ appeared to be areas where high buildings such as apartment housing complexes away from the main road are located. The areas with higher than 2 ℃ SUHI intensity had increased overall and most of the areas with SUHI in the range 2–4 ℃ appeared on the main road and its surrounding areas, in non-apartment housing complexes. Areas with more than 4°C were mostly found in non-apartment housing complexes, industrial complexes, and large scale residential and commercial complex site under construction.

In the case of Pangyo new town, the areas with the SUHI phenomenon increased by approximately 6.5%, and most of these were distributed across the built main road and surrounding areas. The areas with SUHI occurrence in the range 2-4 ℃ increased from 1.77 km^2 (10.06%) to 3.23 km^2 (18.33%) and appeared in the constructed main roads and the surrounding areas. The areas with more than 4 °C were less than 0.324 km^2 (2%) (Fig. 3c).

In 2018, For Bundang new town, the areas with SUHI in the range 0- 2 ℃ had slightly decreased and 2-4 ℃ intensity appeared in most of the apartment complexes. The areas with SUHI in the range 4–6 ℃ increased from 2.76 km^2 (8.25%) to 3.69 km^2 (11.03%) and most of these areas appeared in non-apartment complexes. The areas with more than 6 ℃ increased to approximately 2% of the entire new town and these areas appeared in non-apartment complexes or commercial areas. This implied that the increase in building density and building renovation through additional development may be the main causes of the intensified SUHI phenomenon in existing cities (Fig. 3c). In the case of large scale residential and commercial complex sites, after completion, the structure changed to the same structure as the apartment complex, and the overall SUHI intensity decreased significantly.

In the case of Pangyo new town, the areas experiencing the SUHI phenomenon increased by approximately 17% after the new town development is over. The areas with SUHI occurrence in the range 2–4 ℃ increased from 3.23 km^2 (18.33%) to 4.68 km^2 (26.58%) and most of these areas appeared in apartment complexes like Bundang new town. The areas with SUHI in the range 4–6 ℃ significantly increased from 0.32 km^2 (1.81%) to 2.51 km^2 (14.23%). This is because the proportion of non-apartment housing complexes in the development plan is higher than that of Bundang new town. However, few areas were found that had temperatures greater than 6 °C, and none exceeded 8 °C.

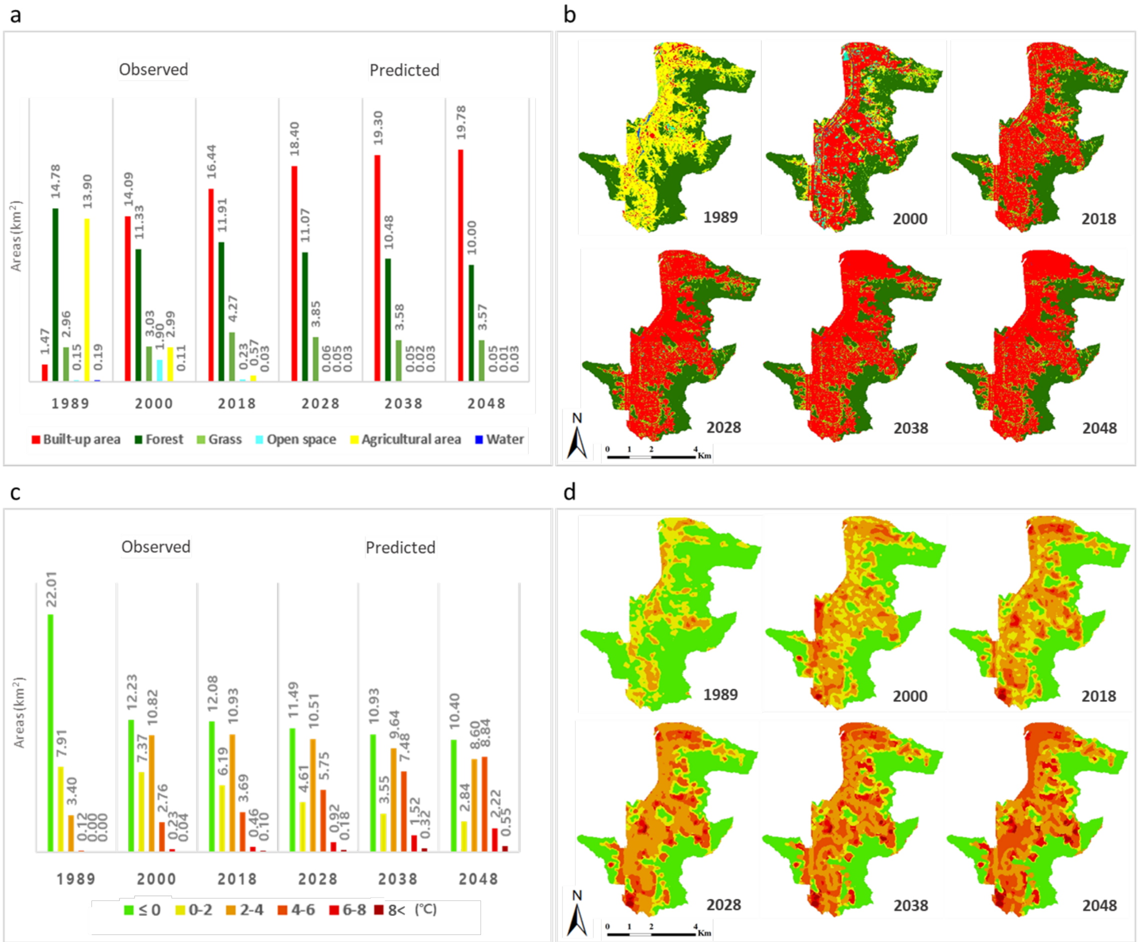

Fig. 2 SUHI distribution according to LULC changes from 1989 to 2048 in Bundang new town. a. Areas of LULC in Bundang new town from 1989 to 2048. **b**. LULC maps of Bundang new town from 1989 to 2048. **c.** Areas of SUHI distribution in Bundang new town from 1989 to 2048. **d**. SUHI distribution maps of Bundang new town from 1989 to 2048.

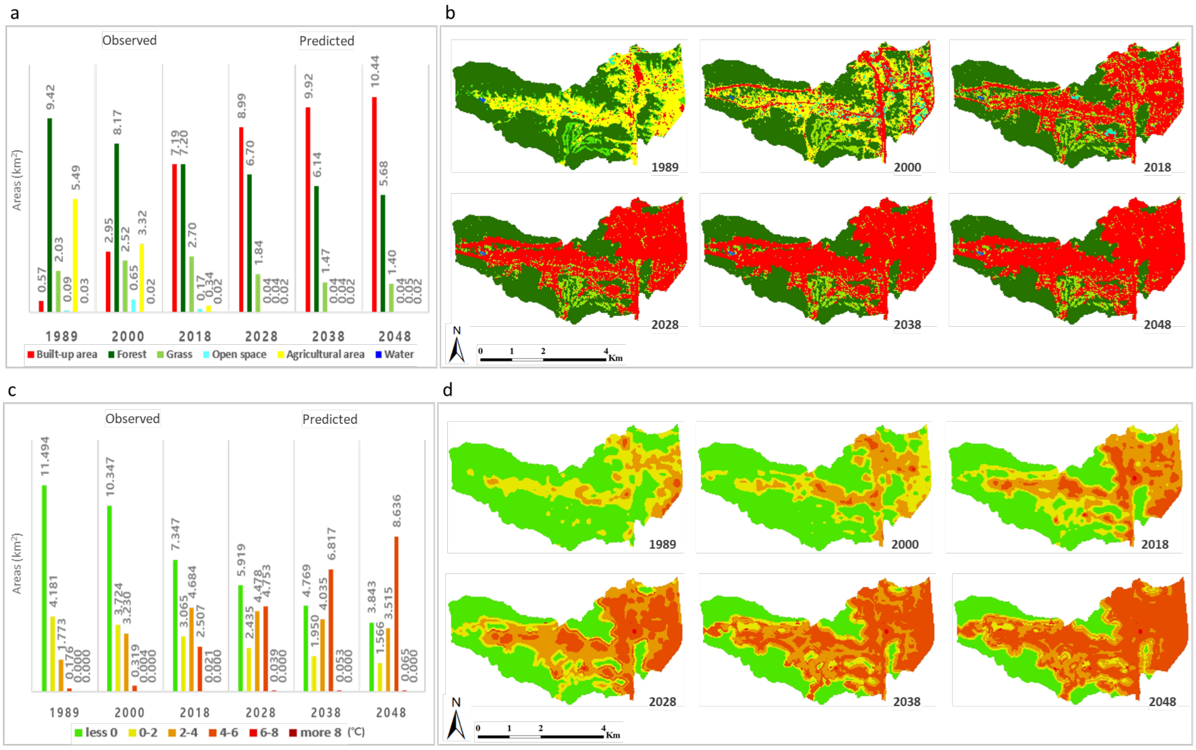

Fig. 3 SUHI distribution according to LULC changes from 1989 to 2048 in Pangyo new town. a. Areas of LULC in Pangyo new town from 1989 to 2048. **b.** LULC maps of Pangyo new town from 1989 to 2048. **c.** Areas of SUHI distribution in Pangyo new town from 1989 to 2048. **d.** SUHI distribution maps of Pangyo new town from 1989 to 2048.

3.3 The relationship between SUHI intensity and urban morphology

Based on the data obtained from National Geographic Information Platform from Ministry of Land, Infrastructure and Transport (MOLIT-NGIP) (http://map.ngii.go.kr/), average building coverage ratio in Bundang new town (27.5%) is higher than Pangyo new town (22.5%) in 2018. Also, the maximum value of the number of buildings per ha was 60 in Bundang new town, which was significantly higher than that value of Pangyo new town, 29. The height of buildings also showed that Bundang new town was high overall, and the max value was 133.5m. On the other hand, in the case of Pangyo new town, there were no buildings with a height of 110m or higher.

According to Oke et al. (2017), the facet surface temperature in daytime in urban system is typically ranked as follows: $T_{roof} > T_{walls} > T_{floor} > T$ surrounding area. In addition, in canyons formed in the city through high-rise buildings, overshadowing areas are formed to induce surface coolness. When vegetation is present, surface cooling becomes stronger due to more shades and transpire. Therefore, if the canyon and roof facets are combined into a single surface temperature for the system, in areas with high vertical building characteristics such as the building height, the SUHI intensity will be lower than other built-up areas. On the other hand, areas with high horizontal building characteristics such as the building coverage ratio or number of buildings, the SUHI intensity will be also high.

Looking at the SUHI intensity distribution of both new towns in 2018, the SUHI intensity in the non-apartment complex consisting of buildings below 4 floors was higher comparing to the apartment complex according to the relationship between the LST and the building structure. This is the reason why the area with SUHI in the range of 4–6 °C increased high in Pangyo new town which the overall height of the buildings is lower than Bundang new town. However, even in the same building complex type, the overall intensity was higher in the Bundang new town, and the areas with SUHI intensity exceeding 6 °C also appeared much more (Fig. 4; Fig. 5). In addition, the SUHI intensity of the apartment complex was also found to be higher overall in the Bundang new town. This is because of the horizontal morphologies such as building coverage ratio and building density of Bundang new town are higher than that of Pangyo new town.

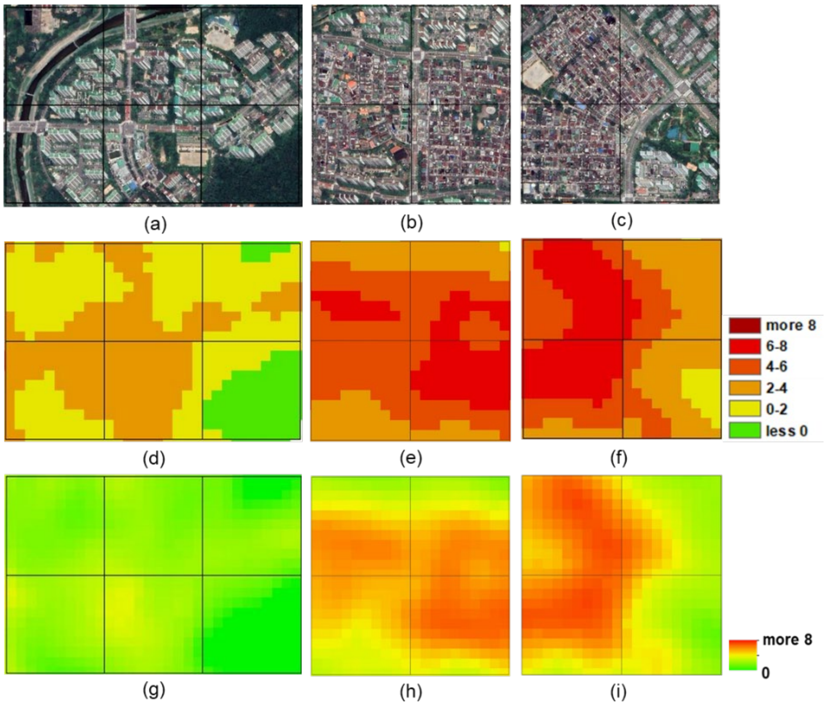

Fig. 4 Site of residential development in Bundang new town (a) high-rise apartment complex, (b) low-rise non-apartment complex 1, (c) low-rise non-apartment complex 2, (d) classified SUHI distribution in high-rise apartment complex, (e) classified SUHI distribution in low-rise non-apartment complex 1, (f) classified SUHI distribution in low-rise non-apartment complex 2, (g) SUHI distribution in high-rise apartment complex, (h) SUHI distribution in low-rise non-apartment complex 1, (i) SUHI distribution in low-rise non-apartment complex 2.

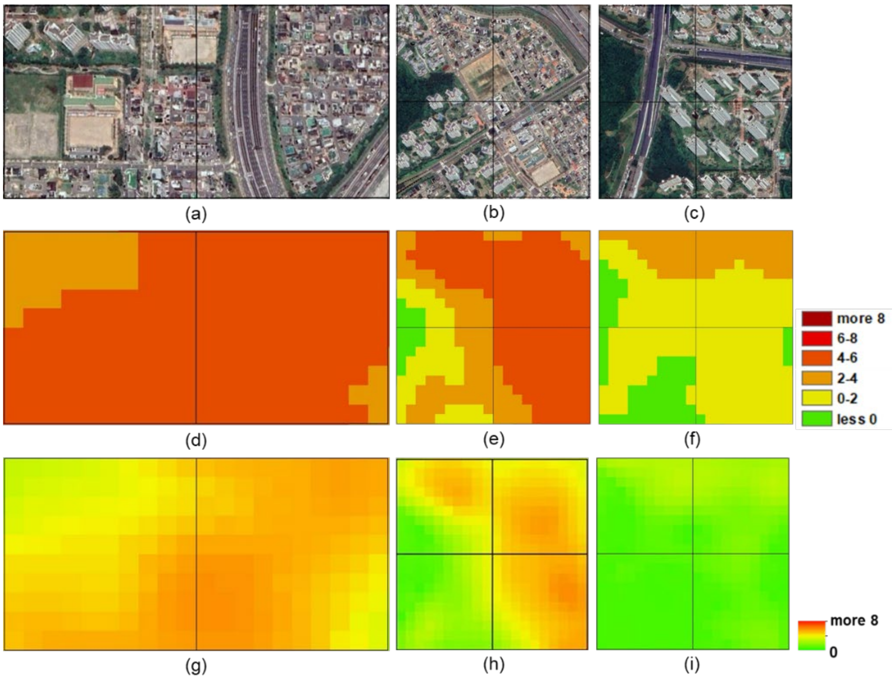

Fig. 5 Site of residential development in Pangyo new town (a) low-rise non-apartment complex, (b) complex buildings, (c) high-rise apartment complex, (d) classified SUHI distribution in low-rise non-apartment complex, (e) classified SUHI distribution in complex buildings, (f) classified SUHI distribution in high-rise apartment complex, (d) SUHI distribution in low-rise non-apartment complex, (e) SUHI distribution in complex buildings, (f) SUHI distribution in high-rise apartment complex.

3.4 Predicted LULC for 2028, 2038 and 2048

The cellular automata (CA)-Markov chain model (MCM) analysis predicted that the proportion of built-up areas would increase by approximately 10% from 16.44 km^2 (49.16%) to 19.78 km^2 (59.12%) between 2018 and 2048 in Bundang new town (Fig. 2a). Moreover, it predicted decreases in forest areas from 11.91 km^2 (35.61%) to 10.0 km^2 (29.9%) and the grass cover from 4.27 km^2 (12.76%) to 3.57 km^2 (10.69%). As a new town development in the past primarily occurred through transformation of agricultural areas to built-up areas, it was not predicted that a significant urban expansion would occur through deforestation. In addition, most of the buildings in the housing complex of Bundang new town were completed in 1990, over 25 years ago. Therefore, renovations are planned for most of these old apartment complexes to improve the poor residential environment and meet the latest urban housing requirements. Hence, most urban expansion was predicted to occur through renovation within the existing built-up areas and partial transformation of the forest surrounding the new town.

In the case of Pangyo new town, the proportion of urban expansion between 2018 and 2048 was predicted to be higher than that of Bundang new town. According to the CA-MCM prediction, built-up areas would increase by approximately 18.42% from 7.19 km^2 (40.81%) to 10.44 km^2 (59.23%), the forest areas would decrease from 7.20 km^2 (40.84%) to 5.68 km^2 (32.25%), and the grass cover including golf courses would decrease from 2.70 km^2 (15.34%) to 1.40 km^2 (7.92%) (Fig. 3a). The primary trend observed in the predicted urban expansion was those non-urban areas, such as forest and grass, surrounding the main road were transformed into built-up areas. In contrast with Bundang new town, Pangyo new town is public-transportation-oriented. During the past new town development, the areas surrounding the main road that existed outside the city were underdeveloped. However, if urban expansion occurs in the future, it would be evident primarily in areas with good road proximity. In addition, urban expansion due to the completion of development in the open spaces that were under development in 2018, and further development within the city was also predicted. In terms of agricultural area and water, both new towns were predicted to remain almost unchanged from 2018, with little fluctuation.

3.5 Predicted SUHI distribution for 2028, 2038, and 2048

The model predicted the increase in area and intensity of the SUHI phenomenon in both new town and unlike LULC prediction, a remarkable change was predicted.

In Bundang new town, the area where the SUHI phenomenon occurs will increase by about 5% between 2018 and 2048. For SUHI intensity distribution, the areas with SUHI 4℃ or less will decrease from 17.12 km^2 (51.16%) to 11.44 km^2 (34.21%). At the same time, the areas with more than SUHI 4℃ was projected to rise from 4.25 km^2 (12.73%) to 10.68 km^2 (34.71%) at the cost of lower SUHI intensity areas. It is predicted that SUHI intensity will expand and increase centering on the existing residential area, which is judged to reflect the trend of renovation and additional building construction that partially occurred between 2000 and 2018. In addition, the areas with more than SUHI 6 ℃ will increase from 0.56 km^2 (1.7%) to 2.77 km^2 (8.28%) and it has been observed that the higher the LST, the higher the frequency of heat waves at regional scales (Fig. 2c) (Yeh et al., 2018). In the future, additional thermal environmental policies and energy policies are needed for areas where SUHI intensity is expected to increase extremely.

In the case of Pangyo new town, the areas where the SUHI phenomenon will occur were predicted to increase by 20%. The affected areas are like those that were predicted to change from forests existing around main road to built-up areas. For SUHI intensity distribution, the area with SUHI 4℃ or less will decrease from 7.75 km^2 (43.97%) to 5.08 km^2 (28.83%). The areas with more than SUHI 4 ℃ was projected to rise from 2.53 km^2 (14.34%) to 8.7 km^2 (49.36%) and most areas were in the range 4-6 ℃ (49%) (Fig. 3c). It can be predicted that as with the Bundang new town, the building density and building coverage ratio are expected to increase through vertical and horizontal renovation and additional construction.

4. Discussion

This study is the first attempt to simulate and compare the pattern of SUHI occurrence according to new towns development using remote sensing and GIS technology. This discussion focuses on the principal two contributions of the proposed research in comparison with previous studies. Afterwards, the limitations are discussed.

The main contribution of our study is that the different patterns of changes in land use land cover and SUHI phenomenon depending on urban planning were visually and quantitatively shown for the study sites excluding external influences. To provide some examples, Tran et al. (2006) and Clinton & Gong (2013) do comparative analysis of SUHI phenomenon between cities under different environment or urban situation. Tran et al. (2006) examines the spatial patterns of SUHIs for Asian mega cities based on the season and relationship with surface properties. Clinton & Gong (2013) estimate the magnitude of SUHI for urban areas between latitudes 71 and – 55 for the year 2010 using MODIS datasets. The results of these studies were successful in demonstrating the contribution of urbanization to the SUHI effect as well as investigating the differences in SUHI between urban and surrounding areas. However, applying these methods could not provide insight into the effect of different urban development types or urban planning on UHI phenomenon. In addition, in terms of comparing the UHI phenomenon between cities, there were some limitations which may lower the reliability of comparison. They all used satellite images constructed at different times and the magnitude of SUHI depends on whether a single image or composite over a period is used (Oke et al., 2017).

In comparison with these previous studies, this research provides a significant contribution by quantifying the influence of the urban planning involved in the UHI phenomenon based on a scientific approach in condition which external influences are controlled. The developed LULC maps showed significant changes in LULC before and after the development of both new towns from 1989 to 2018. The primary driver for the development of both the new towns was the transformation of agricultural areas to built-up areas. Moreover, the increase in built-up areas evidently intensified the SUHI phenomenon of an entire new town. However, the areas where the SUHI phenomenon additionally occurred or the SUHI intensity increased, were different according to the urban plan and morphology.

In the previous surface temperature study in Changwon City in South Korea using remote sensing data and surface measurement, the average temperature of the low-rise housing complex was up to 8 °C higher than that of the high-rise apartment depending on the time (Song & Park, 2017). Three-dimensional urban planning and design considering the effects of both shadow and wind at the same time are required to improve the thermal environment of the housing complex. First, check the weather conditions of each urban area, such as average wind speed, wind direction, and relative humidity, rather than a collective urban plan. Next, establish an individual city plan that is in harmony with the weather condition considering the current parcel division, urban structural condition, and overall building capacity of the city. In the case of building layout, the wind corridor formed by the parallel type layouts is usually beneficial to air flow, creating a good wind environment at pedestrian level (Jiang et al., 2020; Moonen et al., 2011). Also, according to urban planning of each new town, the average greenspace ratio of Pangyo new town had twice that of Bundang new town, which also influenced SUHI intensity. Building a green space is widely suggested strategy to reduce UHI phenomenon. In this way, planting vegetation along the street can contribute to a significant reduction in radiation temperatures rather than planting the same amount of vegetation in a specified green space (Bochenek & Klemm, 2021).

Our research also improves on the predictive models previously developed to study and predict usually LULC patterns. Unlike previous studies, Cellular Automata Markov Chain model was used for prediction of LULC changes and SUHI distribution changes accordingly in study areas. In many previous studies, the LULC change was simply predicted using the CA-MCM model, but overlooked the environmental impact caused by LULC change (Hamad et al., 2018; Kumar et al., 2014; Wang et al., 2021). Saha et al. (2020) and Tariq and Shu (2020) tried to examine the LST change according to the LULC change. However, it did not predict the change of the LST distribution according to the predicted future LULC, and as in previous studies, indirect prediction was performed by simply constructing a regression equation using the spectral index. In addition, the LST value may vary depending on the radiative and aerodynamic properties of the satellite image and it is difficult to confirm the relative temperature increase in the built-up areas according to urban growth using LST distribution (Oke et al., 2017). In this study, the predicted results based on variations between 2000 and 2018 also showed a possible future pattern of further urban expansion and similar changes in SUHI distribution and intensity in both new towns. Changes in the building complex type of future urban areas or horizontal morphology such as urban density and coverage ratio can be inferred from the predicted SUHI intensity trends. Previous studies confirmed a ~~direct~~ linear relationship between building density and UHI intensity and predicted an increase in urban temperature due to urban expansion and densification (Argüeso et al., 2014; Cao et al., 2018; Li et al., 2020; Straka & Sodoudi, 2019). Our results also showed the increase and expansion of SUHI intensity according to urban expansion, which is consistent with the previous studies.

In addition, through prediction analysis, the importance of building renovation and structural characteristics in urban-level thermal environment changes was also suggested. When renovating old buildings in the future, sustainable renovation methods such as increasing the insulation of facades with new surfaces are required to minimize changes in the thermal environment. Height of buildings also need to be considered reducing solar irradiation by shading effects (Loibl et al., 2021).

5. Conclusion

This study suggested a comprehensive approach combining LULC classification, LST analysis and CA-MCM using LANDSAT data for analysis of the current status and future changes of the SUHI phenomenon. Results from this research provide an effective methodology for examine changes in SUHI intensity according to urban planning and morphology. It is easy to apply for practitioners and the necessary data for application are available without complex acquisition procedures as open access datasets. Therefore, the proposed novel method may be applied to both existing and newly built cities to predict future SUHI distribution according to urban planning.

Furthermore, the methods and findings constructed through this research can be helpful to policy makers, urban planners, researchers, and communities by providing a scientific source for thermally sustainable urban planning and morphology. Especially, it was possible to confirm the difference in SUHI intensity and distribution according to the construction of housing complexes with different vertical and horizontal morphology and density. Without effective mitigation, the built-up area in both new towns are estimated to increase to approximately 60%, and the SUHI intensity in most areas to increase up to 4 °C by 2048. Urban areas with the higher the horizontal morphology such as building density and building coverage ratio show higher the SUHI intensity. When the overall height of buildings was lowered for low-density development, SUHI intensity could be increased due to the reduced shading effects. Based on this findings, differential thermal environment management strategies can be analyzed and constructed according to the type of housing complex.

While the presented study provides useful methods and information regarding the current and future status of the UHI phenomenon, it still faces some limitations. This study did not consider a few parameters influencing typical urbanization, including socio-economics factors. Although planned urban expansion has less complicated in terms of physical and legal aspects, typical urban expansion is significantly influenced by the factors such as the complexity of the terrain, degree of socio-economic development, urban regulations, etc (Wang et al., 2021). Therefore, it is necessary to consider additional urban expansion factors when applying this methodology to a region other than new towns. In addition, a model that explains the complex behavior of UHI using a combination of building renovation and especially vertical structural characteristics is still necessary.

In the future, employing the Computational Fluid Dynamic (CFD) model will explain the difference of UHI patterns based on structural characteristics changed by urban planning and building renovation in building scale. Surface temperature measurement will be required to the verification and calibration of the CFD model. The data can be employed for evaluating the methodology used in this study. In addition, the difference in Physiological Equivalent Temperature (PET) by the building morphology could be identified.

Data availability

Satellite images from 1989 to 2018 used in this study are freely available at httl://earthexplorer.usgs.gov/. Other datasets are available upon request from K. Lee (leedake@korea.ac.kr).

References

Aaviksoo, K. (1995). Simulating vegetation dynamics and land use in a mire landscape using a Markov model. *Landscape and Urban Planning*, 31(1-3), 129-142. https://doi.org/10.1016/0169-2046(94)01045-A.

Anas, A., Arnott, R., & Small, K. A. (1998). Urban spatial structure. *Journal of economic literature*, 36(3), 1426-1464. https://www.jstor.org/stable/2564805.

Argüeso, D., Evans, J.P., Fita, L., & Bormann, K. J. (2014). Temperature response to future urbanization and climate change. *Climate dynamics*, 42(7-8), 2183-2199. https://doi.org/10.1007/s00382-013-1789-6.

Artis, D. A., & Carnahan, W. H. (1982). Survey of emissivity variability in thermography of urban areas. *Remote sensing of Environment*, 12(4), 313-329. https://doi.org/10.1016/0034-4257(82)90043-8.

Avdan, U., & Jovanovska, G. (2016). Algorithm for automated mapping of land surface temperature using LANDSAT 8 satellite data. *Journal of sensors, 2016*. https://doi.org/10.1155/2016/1480307.

Bhatti, S. S., & Tripathi, N. K. (2014). Built-up area extraction using Landsat 8 OLI imagery. *GIScience & remote sensing*, 51(4), 445-467. https://doi.org/10.1080/15481603.2014.939539.

Bochenek, A. D., & Klemm, K. (2021). Effectiveness of Tree Pattern in Street Canyons on Thermal Conditions and Human Comfort. Assessment of an Urban Renewal Project in Historical District in Lodz (Poland). *Atmosphere*, 12(6), 751. https://doi.org/10.3390/atmos12060751.

Brown, D. G., Walker, R., Manson, S., & Seto, K. (2004). Modeling land use and land cover change in land change science. *Remote Sens Digit Image Process* (pp. 395–409). Springer, Dordrecht.

Cao, Q., Yu, D., Georgescu, M., Wu, J., & Wang, W. (2018). Impacts of future urban expansion on summer climate and heat-related human health in eastern China. *Environment international*, 112, 134-146. https://doi.org/10.1016/j.envint.2017.12.027.

Carlson, T. N., & Ripley, D. A. (1997). On the relation between NDVI, fractional vegetation cover, and leaf area index. *Remote sensing of Environment*, 62(3), 241-252. https://doi.org/10.1016/S0034-4257(97)00104-1.

Cetin, M. (2015). Determining the bioclimatic comfort in Kastamonu City. *Environmental monitoring and assessment*, 187(10), 1-10. http://doi.org/10.1007/s10661-015-4861-3.

Cetin, M. (2019). The effect of urban planning on urban formations determining bioclimatic comfort area's effect using satellitia imagines on air quality: a case study of Bursa city. *Air Quality, Atmosphere & Health*, 12(10), 1237-1249. https://doi.org/10.1007/s11869-019-00742-4.

Clinton, N., & Gong, P. (2013). MODIS detected surface urban heat islands and sinks: Global locations and controls. *Remote Sensing of Environment*, 134, 294-304. https://doi.org/10.1016/j.rse.2013.03.008.

Congalton, R. G. (1991). A review of assessing the accuracy of classifications of remotely sensed data. *Remote sensing of environment*, 37(1), 35-46. https://doi.org/10.1016/0034-4257(91)90048-B.

Eliasson, I. (2000). The use of climate knowledge in urban planning. *Landscape and urban planning*, 48(1-2), 31-44. https://doi.org/10.1016/S0169-2046(00)00034-7.

Erbek, F. S., Özkan, C., & Taberner, M. (2004). Comparison of maximum likelihood classification method with supervised artificial neural network algorithms for land use activities. *International Journal of Remote Sensing*, 25(9), 1733-1748. https://doi.org/10.1080/0143116031000150077.

Grimmond, S. U. (2007). Urbanization and global environmental change: local effects of urban warming. *Geographical Journal*, 173(1), 83-88. https://doi.org/10.1111/j.1475-4959.2007.232_3.x.

Guha, S., Govil, H., Dey, A., & Gill, N. (2018). Analytical study of land surface temperature with NDVI and NDBI using Landsat 8 OLI and TIRS data in Florence and Naples city, Italy. *European Journal of Remote Sensing*, 51(1), 667-678. https://doi.org/10.1080/22797254.2018.1474494.

Hamad, R., Balzter, H., & Kolo, K. (2018). Predicting land use/land cover changes using a CA-Markov model under two different scenarios. *Sustainability*, 10(10), 3421. https://doi.org/10.3390/su10103421.

Hu, Z., & Lo, C. P. (2007). Modeling urban growth in Atlanta using logistic regression. *Computers, environment and urban systems*, 31(6), 667-688. https://doi.org/10.1016/j.compenvurbsys.2006.11.001.

Jiang, Y., Wu, C., & Teng, M. (2020). Impact of Residential Building Layouts on Microclimate in a High Temperature and High Humidity Region. *Sustainability*, 12(3), 1046. https://doi.org/10.3390/su12031046.

Kamusoko, C., Aniya, M., Adi, B., & Manjoro, M. (2009). Rural sustainability under threat in Zimbabwe–simulation of future land use/cover changes in the Bindura district based on the Markov-cellular automata model. *Applied Geography*, 29(3), 435-447. https://doi.org/10.1016/j.apgeog.2008.10.002.

Kasraian, D., Maat, K., & van Wee, B. (2019). The impact of urban proximity, transport accessibility and policy on urban growth: A longitudinal analysis over five decades. *Environment and Planning B: Urban Analytics and City Science*, 46(6), 1000-1017. https://doi.org/10.1177/2399808317740355.

Kechebour, B. E. (2015). Relation between stability of slope and the urban density: case study. *Procedia Engineering*, 114, 824-831. https://doi.org/10.1016/j.proeng.2015.08.034.

Kumar, S., Radhakrishnan, N., & Mathew, S. (2014). Land use change modelling using a Markov model and remote sensing. *Geomatics, Natural Hazards and Risk*, 5(2), 145-156. https://doi.org/10.1080/19475705.2013.795502.

Lee, K., Sung, H. C., Seo, J. Y., Yoo, Y., Kim, Y., Kook, J. H., & Jeon, S. W. (2020). The Integration of Remote Sensing and Field Surveys to Detect Ecologically Damaged Areas for Restoration in South Korea. *Remote Sensing*, 12(22), 3687. https://doi.org/10.3390/rs12223687.

Lee, K., Kim, Y., Sung, H. C., Ryu, J., & Jeon, S. W. (2020). Trend analysis of urban heat island intensity according to urban area change in Asian mega cities. *Sustainability*, 12(1), 112. https://doi.org/10.3390/su12010112.

Li, Y., Schubert, S., Kropp, J. P., & Rybski, D. (2020). On the influence of density and morphology on the Urban Heat Island intensity. *Nature communications*, 11(1), 1-9. https://doi.org/10.1038/s41467-020-16461-9.

Liping, C., Yujun, S., & Saeed, S. (2018). Monitoring and predicting land use and land cover changes using remote sensing and GIS techniques—A case study of a hilly area, Jiangle, China. *PloS one*, 13(7), e0200493. https://doi.org/10.1371/journal.pone.0200493.

Loibl, W., Vuckovic, M., Etminan, G., Ratheiser, M., Tschannett, S., & Österreicher, D. (2021). Effects of Densification on Urban Microclimate—A Case Study for the City of Vienna. *Atmosphere*, 12(4), 511. https://doi.org/10.3390/atmos12040511.

Mallick, J., Singh, C. K., Shashtri, S., Rahman, A., & Mukherjee, S. (2012). Land surface emissivity retrieval based on moisture index from LANDSAT TM satellite data over heterogeneous surfaces of Delhi city. *International Journal of Applied Earth Observation and Geoinformation*, 19, 348-358. https://doi.org/10.1016/j.jag.2012.06.002.

Moonen, P., Dorer, V., & Carmeliet, J. (2011). Evaluation of the ventilation potential of courtyards and urban street canyons using RANS and LES. *Journal of Wind Engineering and Industrial Aerodynamics*, 99(4), 414-423. https://doi.org/10.1016/j.jweia.2010.12.012.

Myint, S. W., & Wang, L. (2006). Multicriteria decision approach for land use land cover change using Markov chain analysis and a cellular automata approach. *Canadian Journal of Remote Sensing*, 32(6), 390-404. https://doi.org/10.5589/m06-032.

Nations, U. (2018). *The World's cities in 2018*. Department of Economic and Social Affairs, Population Division, World Urbanization Prospects.

Nazeer, M., Nichol, J. E., & Yung, Y. K. (2014). Evaluation of atmospheric correction models and Landsat surface reflectance product in an urban coastal environment. *International journal of remote sensing*, 35(16), 6271-6291. https://doi.org/10.1080/01431161.2014.951742.

Oke, T. R. (2002). *Boundary layer climates*. Routledge.

Oke, T. R., Mills, G., Christen, A., & Voogt, J. A. (2017). *Urban climates*. Cambridge University Press.

Qaid, A., Lamit, H. B., Ossen, D. R., & Shahminan, R. N. R. (2016). Urban heat island and thermal comfort conditions at micro-climate scale in a tropical planned city. *Energy and Buildings*, 133, 577-595. https://doi.org/10.1016/j.enbuild.2016.10.006.

Radhi, H., Fikry, F., & Sharples, S. (2013). Impacts of urbanisation on the thermal behaviour of new built up environments: A scoping study of the urban heat island in Bahrain. *Landscape and Urban Planning*, 113, 47-61. https://doi.org/10.1016/j.landurbplan.2013.01.013.

Raymond, W. H., Rabin, R. M., & Wade, G. S. (1994). Evidence of an agricultural heat island in the lower Mississippi River floodplain. Bulletin of the American Meteorological Society, 75(6), 1019–1026. https:// doi. org/ 10.1175/ 1520- 0477(1994) 075< 1019: EOAAH I>2. 0. CO;2

Saha, P., Bandopadhyay, S., Kumar, C., & Mitra, C. (2020). Multi-approach synergic investigation between land surface temperature and land-use land-cover. *Journal of Earth System Science*, 129(1), 1-21. https://doi.org/10.1007/s12040-020-1342-z.

Sang, L., Zhang, C., Yang, J., Zhu, D., & Yun, W. (2011). Simulation of land use spatial pattern of towns and villages based on CA–Markov model. *Mathematical and Computer Modelling*, 54(3-4), 938-943. https://doi.org/10.1016/j.mcm.2010.11.019.

Santamouris, M. (2013). Using cool pavements as a mitigation strategy to fight urban heat island—A review of the actual developments. *Renewable and Sustainable Energy Reviews*, 26, 224-240. https://doi.org/10.1016/j.rser.2013.05.047.

Straka, M., & Sodoudi, S. (2019). Evaluating climate change adaptation strategies and scenarios of enhanced vertical and horizontal compactness at urban scale (a case study for berlin). *Landscape and Urban Planning*, 183, 68-78. https://doi.org/10.1016/j.landurbplan.2018.11.006.

Sekertekin, A., & Bonafoni, S. (2020). Land surface temperature retrieval from Landsat 5, 7, and 8 over rural areas: assessment of different retrieval algorithms and emissivity models and toolbox implementation. *Remote Sensing*, 12(2), 294. https://doi.org/10.3390/rs12020294.

Shen, H., Huang, L., Zhang, L., Wu, P., & Zeng, C. (2016). Long-term and fine-scale satellite monitoring of the urban heat island effect by the fusion of multi-temporal and multi-sensor remote sensed data: A 26-year case study of the city of Wuhan in China. *Remote Sensing of Environment*, 172, 109-125. https://doi.org/10.1016/j.rse.2015.11.005.

Sobrino, J. A., & Raissouni, N. (2000). Toward remote sensing methods for land cover dynamic monitoring: Application to Morocco. *International journal of remote sensing*, 21(2), 353-366. https://doi.org/10.1080/014311600210876.

Sobrino, J. A., Jiménez-Muñoz, J. C., & Paolini, L. (2004). Land surface temperature retrieval from LANDSAT TM 5. *Remote Sensing of environment*, 90(4), 434-440. https://doi.org/10.1016/j.rse.2004.02.003.

Song, B.G., & Park, K.H. (2017). Comparison of ASTER Satellite and Ground-Based Surface. *Journal of the Korean Association of Geographic Information Studies*, 20(3), 104-124 (in Korean with English abstract). https://doi.org/10.11108/kagis.2017.20.3.104.

Sun, J., Yang, J., Zhang, C., Yun, W., & Qu, J. (2013). Automatic remotely sensed image classification in a grid environment based on the maximum likelihood method. *Mathematical and Computer Modelling*, 58(3-4), 573-581. https://doi.org/10.1016/j.mcm.2011.10.063.

Sun, H., Chen, Y., & Zhan, W. (2015). Comparing surface-and canopy-layer urban heat islands over Beijing using MODIS data. *International Journal of Remote Sensing*, 36(21), 5448-5465. https://doi.org/10.1080/01431161.2015.1101504.

Tariq, A., & Shu, H. (2020). CA-Markov Chain Analysis of Seasonal Land Surface Temperature and Land Use Land Cover Change Using Optical Multi-Temporal Satellite Data of Faisalabad, Pakistan. *Remote Sensing*,

12(20), 3402. https://doi.org/10.3390/rs12203402.
Tran, H., Uchihama, D., Ochi, S., & Yasuoka, Y. (2006). Assessment with satellite data of the urban heat island effects in Asian mega cities. *International journal of applied Earth observation and Geoinformation*, 8(1), 34-48. https://doi.org/10.1016/j.jag.2005.05.003.
Tucker, C. J. (1979). Red and photographic infrared linear combinations for monitoring vegetation. *Remote sensing of Environment*, 8(2), 127-150. https://doi.org/10.1016/0034-4257(79)90013-0.
Voogt, J. A., & Oke, T. R. (2003). Thermal remote sensing of urban climates. *Remote sensing of environment*, 86(3), 370-384. https://doi.org/10.1016/S0034-4257(03)00079-8.
Wakeman, R. (2016). *Practicing utopia: an intellectual history of the new town movement*. University of Chicago Press.
Wang, F., & Ge, Q. (2012). Estimation of urbanization bias in observed surface temperature change in China from 1980 to 2009 using satellite land-use data. *Chinese Science Bulletin*, 57(14), 1708-1715. https://doi.org/10.1007/s11434-012-4999-0.
Wang, F., Qin, Z., Song, C., Tu, L., Karnieli, A., & Zhao, S. (2015). An improved mono-window algorithm for land surface temperature retrieval from Landsat 8 thermal infrared sensor data. *Remote sensing*, 7(4), 4268-4289. https://doi.org/10.3390/rs70404268.
Wang, S. W., Munkhnasan, L., & Lee, W. K. (2021). Land use and land cover change detection and prediction in Bhutan's high altitude city of Thimphu, using cellular automata and Markov chain. *Environmental Challenges*, 2, 100017.
Weng, Q., Lu, D., & Schubring, J. (2004). Estimation of land surface temperature–vegetation abundance relationship for urban heat island studies. *Remote sensing of Environment*, 89(4), 467-483. https://doi.org/10.1016/j.envc.2020.100017.
Yu, X., Guo, X., & Wu, Z. (2014). Land surface temperature retrieval from Landsat 8 TIRS—Comparison between radiative transfer equation-based method, split window algorithm and single channel method. Remote Sensing, 6(10), 9829–9852. https:// doi. org/ 10. 3390/ rs610 9829
Zha, Y., Gao, J., & Ni, S. (2003). Use of normalized difference built-up index in automatically mapping urban areas from TM imagery. *International journal of remote sensing*, 24(3), 583-594. https://doi.org/10.1080/01431160304987.
Zhou, B., Rybski, D., & Kropp, J. P. (2013). On the statistics of urban heat island intensity. *Geophysical research letters*, 40(20), 5486-5491. https://doi.org/10.1002/2013GL057320.

Acknowledgements

This work was conducted with the support of the Korea Environment Industry & Technology Institute (KEITI) through its Urban Ecological Health Promotion Technology Development Project and funded by the Korea Ministry of Environment (MOE) (2020002770003).

Author contributions

K. Lee, S.H. Kim, and S.W. Jeon: research design; H.C. Sung and Y. Kim: data collection; K. Lee, Y. Kim, and H.C. Sung: empirical analysis; K. Lee and S.H. Kim: manuscript draft; and all authors: result interpretation and writing the paper.

Declaration of Competing Interest

The authors declare no competing interests.